BROADBAND 4×4 NON-BLOCKING OPTICAL SWITCH FABRIC BASED ON MACH-ZEHNDER INTERFEROMETERS

Linjie Zhou, Liangjun Lu, Zuxiang Li, and Jianping Chen*

State Key Laboratory of Advanced Optical Communication Systems and Networks
Department of Electronic Engineering, Shanghai Jiao Tong University, Shanghai 200240, China
Email: ljzhou@sjtu.edu.cn

ABSTRACT

We demonstrate a silicon 4×4 non-blocking Benes switch fabric consisting of three stages of tunable Mach-Zehnder interferometers. Measurements show that the insertion loss is around 10 dB and the crosstalk is below -10 dB over a 40 nm wide wavelength range.

Keywords: *Silicon photonics, Optical switches, Mach-Zehnder interferometers*

1. INTRODUCTION

An optical switch fabric is essential for optical signal routing in optical communications and photonic networks-on-chip (NoC) [1]. A variety of technologies have been employed to implement optical switches, among which the micro-electro-mechanical systems (MEMS) [2] and silica planar lightwave circuits (PLC) [3] based switches are most well developed. The MEMS technology allows for easy scalability to a large port count, small wavelength and polarization dependence, and loss crosstalk. The PLC is also a viable technology for large-scale optical switches owning to its low loss, planar integration, and easy coupling with optical fibers. However, both of these technologies have the common shortcomings, such as large footprint, high power consumption, and low tuning speed (in the millisecond to the microsecond range), which greatly limits their broad applications.

With the emergence of silicon photonics technology, various passive and active optical components can be monolithically integrated on one silicon chip together with the electronic driver circuits [4-8], making it possible to realize optical switches based on silicon waveguide systems. Silicon waveguides have very small cross-sectional dimensions and bending radii, enabling a very compact device size. Meanwhile, the high-speed free carrier plasma dispersion effect (FCD) can provide a tuning speed as fast as 10's GHz. The CMOS compatible fabrication of silicon photonics devices also offers the potential for high-volume and low-cost production.

A N×N switch fabric is usually composed of multiple 2×2 switch building blocks. Single or coupled microring resonators can be used as the basic switching elements [9-11]. Previously, we demonstrated Mach-Zehnder interferometer (MZI) coupled microring resonators to work as optical switches where electrical tuning is either applied to the MZI arm or to the microrings [10, 11]. The microring-based schemes have the advantages of high compactness and low tuning power. However, their narrow optical bandwidth and high sensitivity to fabrication errors and environmental temperature variations limit their practical usage. Another commonly used switching element is the symmetric MZI structure, featuring broadband operation and high robustness [12-14]. Compared to the microring, the MZI needs a larger phase shift to change the switching state. Given the strong FCD effect, it is possible to shift π phase using a p-i-n diode in a modulation arm as short as a few 100 μm upon a small forward bias.

Here we report a broadband 4×4 non-blocking optical switch using MZIs as its building blocks in a Benes architecture. Each MZI is integrated with both electro-optic (EO) and thermo-optic (TO) electrodes for convenient fast switch and phase compensation, respectively. Preliminary experimental results are presented.

2. DEVICE DESIGN AND FABRICATION

Figure 1(a) shows the 4×4 rearrangeably non-blocking Benes switch fabric. The Benes architecture requires the minimum number of switching elements to obtain the full switch states and lowest insertion loss compared to Crossbar, Clos, Fat-Tree, Torus and other architectures. Only three stages of switching elements are required for the 4×4 Benes architecture. As can be seen, waveguide crossings are necessary to construct the fabric. In order to reduce the insertion loss and crosstalk at each crossing, we design 90^{o}-crossed 1×1 MMIs to utilize the self-imaging principle for the light to cross over the waveguide junction.

Figure 1(b) shows the switching element based on a MZI. The MZI is composed of two 2×2 multimode

interferometers (MMIs) with the arms each integrated with an EO tuning electrode made of a p-i-n diode and a TO tuning electrode made of a silicon resistor [15]. The TO tuning is used to correct phase errors induced by fabrication errors while the EO tuning is used for fast switching in the GHz range. By changing the phase difference of the two arms from 0 to π, the MZI changes the state from "cross" to "bar" that we refer to as "0" and "1", respectively. As each switching element has two states, there are totally 2^6=64 combinations, among switch some are redundant. For non-blocking operation, only 24 permutations are needed.

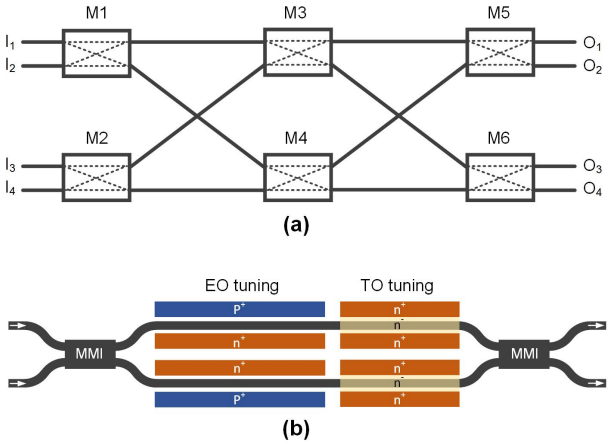

Fig. 1 (a) 4x4 Benes switch architecture. (b) MZI switching element.

The switch is based on silicon-on-insulator (SOI) ridge waveguides with a cross-sectional dimension of 0.5 μm (width) × 0.22 μm (height) and a slab thickness of 0.06 μm. The lengths of the p-i-n diode and the resistive heater are 356 μm and 89 μm, respectively. The highly doped p^+ and n^+ regions have a doping concentration of ~10^{20} cm^{-3}, separated from the waveguide edges by 0.8 μm to avoid free carrier absorption. The lightly doped n^- region in the resistive heater has a doping concentration of ~8×10^{16} cm^{-3} to reduce the resistance while maintaining a low loss for the silicon waveguides. The fabrication was done using CMOS compatible processes.

Figure 2 shows the optical microscope image of the fabricated 4×4 switch. The footprint of the device is 3.5 × 1.4 mm^2. Grating couplers with a 630 nm period and a 70 nm shallow etch depth are used for input and output coupling with a fiber array. It should be noted that the waveguides are elongated before terminated with grating couplers in order to leave enough space for fiber array coupling and wire bonding to signal pads. In our design, we purposely add a directional coupler in each output waveguide so that output light can be routed both to the left side (fiber array coupling) and to the right side (individual fiber coupling) for easy testing. The directional coupler is designed to have a gap of 200 nm and a coupling length of 13 μm. The splitting loss for the fiber array end is about 4.8 dB. The metal pads are finally wire-bonded to a printed circuit board (PCB) so that voltages can be applied onto the p-i-n diodes and the resistive heaters.

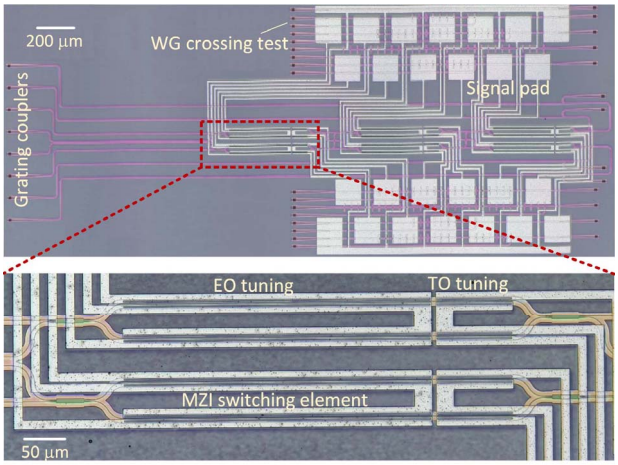

Fig. 2 Optical microscope image of the fabricated 4×4 switch fabric. The inset shows the magnified image of the MZI switching element.

3. EXPERIMENTAL RESULTS

We first characterize the insertion loss of the MMI-based waveguide crossing. Figure 3 shows the wavelength dependent insertion loss of one waveguide crossing. The loss is extracted by linear fitting the accumulative loss of 10, 20, and 30 series-connected crossings. The loss is around 0.17 dB at 1550 nm and reduces at the shorter wavelengths. The fact that the optimal wavelength is not at 1550 nm is probably because of the inaccuracy in our simulation used to design the MMI.

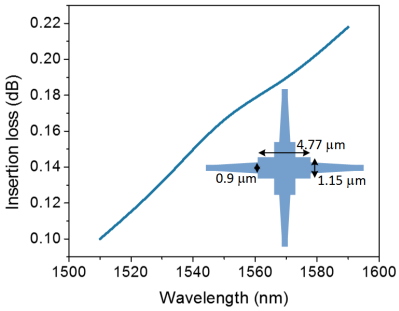

Fig. 3 Measured insertion loss of the MMI-based waveguide crossing. The inset shows the crossing structure.

We then characterize the routing functionality of the switch by using transverse electrically (TE) polarized light from a scanning laser and measuring the transmission spectra. Without tuning, the switching elements are all in the "cross" connection, and we refer to this state as "000000" state. Because of phase errors, the MZI arms are unbalanced for the as-fabricated device. We perform TO tuning for each switching element to correct the phase errors. The TO tuning power consumptions are listed in Table 1. Once the phase errors

are corrected, the TO power is fixed during the following EO tuning to change the switch state.

TABLE I
POWER CONSUMPTION OF THE SWITCHING ELEMENTS

Switching elements	M1	M2	M3	M4	M5	M6
TO (mW)	6	7.2	4	7.6	8.1	0.81
EO (mW)	7.9	8.1	5.8	7.3	4.5	4.9

Figure 4 shows the measured transmission spectra for the "000000" state. In each plot, light is launched from one input port and the spectra from the four output ports are record. The spectra are all normalized to a test waveguide to eliminate the effect of grating couplers. One can see that the input and output ports are mapped as I_1-O_3, I_2-O_4, I_3-O_1, and I_4-O_2 with an insertion loss of around 10 dB. The insertion loss comes from the switching elements, connection waveguides, waveguide crossings, and power splitters. It should be noted the insertion loss slightly decreases with wavelength because the directional coupler has a higher coupling ratio at a longer wavelength. The leakage power to the other three output ports composes the crosstalk to the main routing path. The average crosstalk is around -15 dB. The crosstalk is mainly resulted from the limited extinction ratio of the switching elements. Although we have corrected the phase errors in the MZI arms, the 2×2 MMIs in the MZI may not have a perfect 50:50 splitting ratio, which as a result cannot give 100% transmission at the "cross" state.

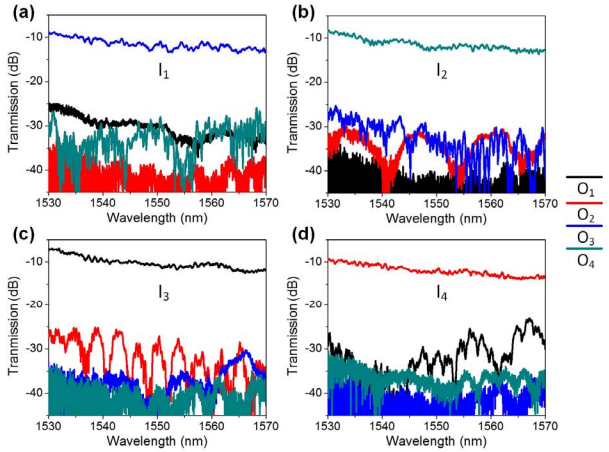

Fig. 4 Spectral characteristics of all signal and crosstalk paths for the 4×4 switch when it is configured as "000000" state with the input from (a) I_1, (b) I_2, (c) I_3, and (d) I_4.

When all switching elements changes from "cross" to "bar" state by introducing a π phase shift in one MZI arm upon tuning on the p-i-n diodes, the switch fabric is configured to the "111111" state. The EO power consumption of each switching element is shown in Table 1 (EO tuning is applied to the MZI bottom arm). Because of the variations in I-V characteristics of the p-i-n diodes, the EO power consumption varies from 4.5 to 8.1 mW. Figure 5 shows the transmission spectra for the "111111" state. As compared to the previous state, the insertion loss increases by a few dB, and the crosstalk deteriorates to around -10 dB. The performance degradation is caused by the excess loss induced during EO tuning. After p-i-n diodes tuned on, not only is the refractive index changed, the waveguide loss is also increased. As a result, the optical power becomes unbalanced in the MZI two arms, giving rise to reduced extinction ratio and hence higher insertion loss and crosstalk. It is also observable that some crosstalk spectra exhibit periodic interference patterns, e.g., I_1-O_2, which manifests the presence of two crosstalk optical paths with comparable power levels.

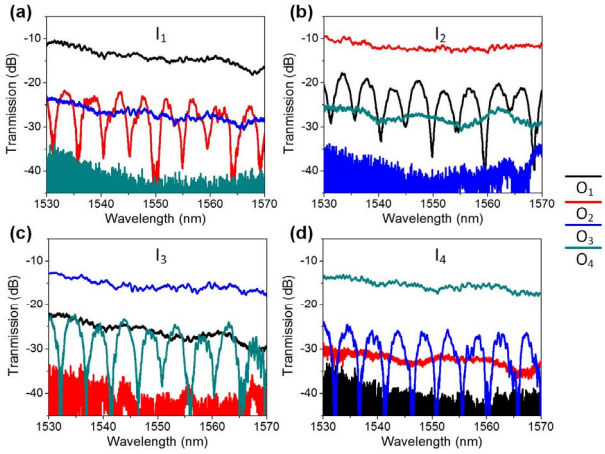

Fig. 5 Spectral characteristics of all signal and crosstalk paths for the 4×4 switch when it is configured as "111111" state with the input from (a) I_1, (b) I_2, (c) I_3, and (d) I_4.

Besides the above two special switching states, our switch fabric can also be conveniently configured to any of the 24 states necessary for non-blocking operation by tuning the EO electrodes. As examples, we turn on half of the EO electrodes to set the states to "100110" and "110100", and the measured spectra are shown in Figs. 6 and 7, respectively. It can be seen that the insertion loss and crosstalk are in between the all "0" and all "1" states, which is understandable since the performances of the switching elements in terms of insertion loss and extinction ratio are degraded once they are turned on.

It should be mentioned that the waveguide loss is inevitably increased during phase modulation, and hence it is difficult to reduce the crosstalk to below -20 dB. In order to solve this issue, more complicated switch units are proposed, for example, using four MZIs to construct the 2×2 switch unit [16]. In this way, the crosstalk can be lowered to less than -30 dB. With this method, the performance of our 2×2 switch fabric can be further improved.

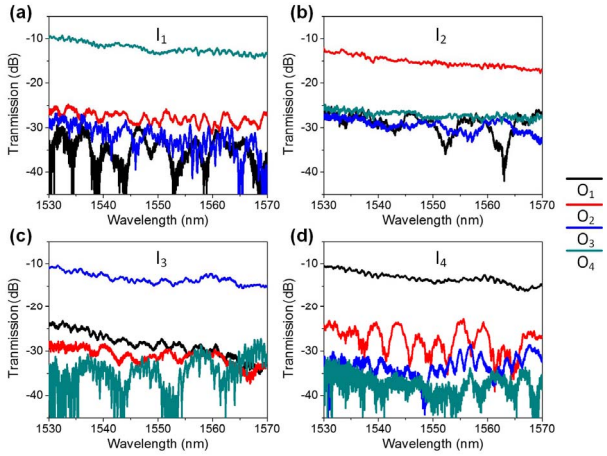

Fig. 6 Spectral characteristics of all signal and crosstalk paths for the 4×4 switch when it is configured as "100110" state with the input from (a) I_1, (b) I_2, (c) I_3, and (d) I_4.

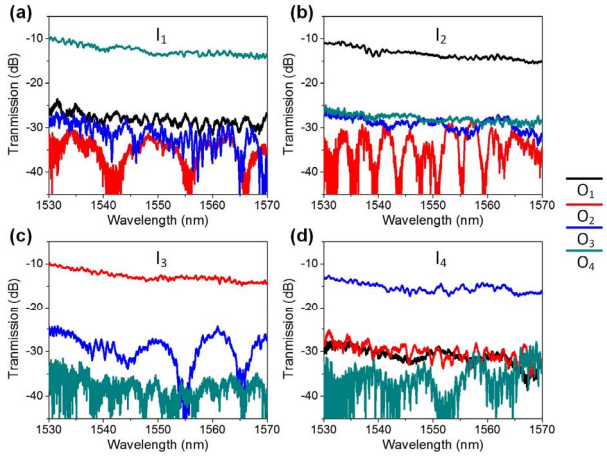

Fig. 7 Spectral characteristics of all signal and crosstalk paths for the 4×4 switch when it is configured as "110100" state with the input from (a) I_1, (b) I_2, (c) I_3, and (d) I_4.

4. CONCLUSION

We have demonstrated a silicon 4×4 non-blocking switch fabric based on a Benes architecture with MZIs as the switching elements. Preliminary experimental results reveal that the switch has insertion loss around 10 dB and crosstalk below -10 dB. The operation is broadband, covering the C band wavelength range.

5. ACKNOWLEDGEMENTS

This work was supported in part by the 973 program (ID2011CB301700), the 863 program (2013AA014402), the National Natural Science Foundation of China (NSFC) (61127016, 61107041), SRFDP of MOE (Grant No. 20130073130005). We also acknowledge IME Singapore for device fabrication.

6. REFERENCES

[1] A. Shacham, K. Bergman, and L. P. Carloni, "Photonic networks-on-chip for future generations of chip multiprocessors," *IEEE Trans. Comp.,* vol. 57, pp. 1246-1260, 2008.

[2] P. De Dobbelaere, K. Falta, S. Gloeckner, and S. Patra, "Digital MEMS for optical switching," *IEEE Comm. Mag.,* vol. 40, pp. 88-95, 2002.

[3] T. Goh, M. Yasu, K. Hattori, A. Himeno, M. Okuno, and Y. Ohmori, "Low-loss and high-extinction-ratio silica-based strictly nonblocking 16/spl times/16 thermooptic matrix switch," *IEEE Photon. Technol. Lett.,* vol. 10, pp. 810-812, 1998.

[4] L. Lu, L. Zhou, X. Sun, J. Xie, Z. Zou, H. Zhu, *et al.*, "CMOS-compatible temperature-independent tunable silicon optical lattice filters," *Opt. Express,* vol. 21, pp. 9447-9456, 2013.

[5] H. Zhu, L. Zhou, X. Sun, Y. Zhou, X. Li, and J. Chen, "On-chip optical power monitor using periodically interleaved PN junctions integrated on a silicon waveguide," *IEEE J. Sel. Top. Quantum Electron.,* vol. 20, p. 3800408, 2014.

[6] B. Guan, S. Djordjevic, N. Fontaine, L. Zhou, S. Ibrahim, R. Scott, *et al.*, "CMOS Compatible Reconfigurable Silicon Photonic Lattice Filters using Cascaded Unit Cells for RF-Photonic Processing," *IEEE J. Sel. Top. Quantum Electron.,* vol. 20, p. 8202110, 2014.

[7] D. J. Lockwood and L. Pavesi, *Silicon Photonics II*: Springer, 2011.

[8] D. Liang and J. E. Bowers, "Recent progress in lasers on silicon," *Nat. Photon.,* vol. 4, pp. 511-517, 2010.

[9] R. Ji, J. Xu, and L. Yang, "Five-port optical router based on microring switches for photonic networks-on-chip," *IEEE Photon. Technol. Lett,* vol. 25, pp. 492-495, 2013.

[10] L. Lu, L. Zhou, X. Li, and J. Chen, "Low-power 2× 2 silicon electro-optic switches based on double-ring assisted Mach–Zehnder interferometers," *Opt. Lett.,* vol. 39, pp. 1633-1636, 2014.

[11] L. Zhou and A. W. Poon, "Fano resonance-based electrically reconfigurable add-drop filters in silicon microring resonator-coupled Mach-Zehnder interferometers," *Opt. Lett.,* vol. 32, pp. 781-783, 2007.

[12] K. Suzuki, K. Tanizawa, T. Matsukawa, G. Cong, S.-H. Kim, S. Suda, *et al.*, "Ultra-compact 8× 8 strictly-non-blocking Si-wire PILOSS switch," *Opt. Express,* vol. 22, pp. 3887-3894, 2014.

[13] B. G. Lee, A. V. Rylyakov, W. M. Green, S. Assefa, C. W. Baks, R. Rimolo-Donadio, *et al.*, "Monolithic silicon integration of scaled photonic switch fabrics, CMOS logic, and device driver circuits," *J. Lightwave Technol.,* vol. 32, pp. 743-751, 2014.

[14] L. Chen and Y.-k. Chen, "Compact, low-loss and low-power 8× 8 broadband silicon optical switch," *Opt. Express,* vol. 20, pp. 18977-18985, 2012.

[15] L. Zhou, X. Zhang, L. Lu, and J. Chen, "Tunable vernier microring optical filters with p-i-p type microheaters," *IEEE Photon. J.,* vol. 5, p. 6601211, 2013.

[16] J. Xing, Z. Li, Y. Yu, and J. Yu, "Low cross-talk 2× 2 silicon electro-optic switch matrix with a double-gate configuration," *Opt. Lett.,* vol. 38, pp. 4774-4776, 2013.